Resonance energy transfer from a cylindrical distribution of donors to a plane of acceptors

Location of apo-B100 protein on the human low-density lipoprotein particle

Philippe Bastiaens, Anthony de Beus, Michael Lacker, Pentti Somerharju,* Matti Vauhkonen,* and Josef Eisinger

Department of Physiology and Biophysics, Mount Sinai School of Medicine, New York 10029 USA; and *Department of Medical Chemistry, University of Helsinki, Helsinki, Finland

ABSTRACT The resonance energy transfer (RET) from a cylindrical assembly of donors to acceptors in a plane was investigated, and the dependence the average RET rate (k_T) on the cylinder's size, shape, and proximity to the acceptor plane was determined. This geometry provides a model for the RET from a donor-containing protein to acceptors embedded in an associated phospholipid mono- or bilayer. The determination of k_T for a series of acceptors at different levels in the phospholipid layer is shown to provide information on the protein's relationship to the phospholipid layer. Two models for the donor (D) and acceptor (A) distributions are employed: (*a*) The D's and A's are uniformly distributed in the cylinder and the plane, respectively, and analytical expressions for k_T in terms of experimental parameters are derived. (*b*) The RET rates between all D, A pairs within the cylinder and in the plane are calculated and averaged for a large number of random D and A distributions. The average transfer rates obtained by the two approaches are in agreement and the width of the frequency distribution of k_T for the latter provides an estimate of the error to be expected when, as is usually the case, the true D and A locations are unknown. This methodology is illustrated by analyzing RET from the 37 tryptophan residues of the apo-B100 protein to a series of pyrenylphosphatidylcholine acceptors inserted in the phospholipid monolayer of the human low-density lipoprotein particle, and it is concluded that significant portions of the protein penetrate the phospholipid layer.

1. INTRODUCTION

Resonance energy transfer (RET) is the mechanism by which the excitation energy of a donor chromophore is transferred nonradiatively to a nearby acceptor molecule. The rate of RET (k_T) was shown by Förster to be a sensitive function of the separation and the relative orientations of the donor and acceptor moieties (Förster, 1948). Therefore, the measurement of k_T provides the experimenter with a practical "spectroscopic ruler" for donor-acceptor separations of up to 10 nm (Stryer, 1978), as long as the donor and acceptor transition moment directions are at least approximately dynamically averaged (Dale et al., 1979). Because distances of this magnitude correspond to the dimensions of many biological structures (e.g., proteins, membranes), RET experiments have, for example, been used to estimate the separation of individual donor-acceptor pairs in hormones (Schiller, 1972) and proteins (Torgerson and Morales, 1984) and to determine the proximity of hemoglobin molecules to the membrane of red blood cells (Eisinger and Flores, 1983; Eisinger et al., 1984).

In this paper, we consider RET from an assembly of donors within a right cylinder to acceptors in a plane parallel to the cylinder's base. This geometry is considered to approximate that of a protein containing many donor chromophores in close proximity to a membrane in which lipid analogue receptors are embedded. It will be shown that within the limitations of this model, energy transfer experiments can provide useful information on the location of a protein with respect to the phospholipid layer it is associated with.

Our analysis is presented in terms of dimensionless parameters to make its results readily applicable to any donor-acceptor pair. The methodology is illustrated by an analysis of the measured RET efficiency from the 37 tryptophan residues of the apo-B100 protein to a series of different pyrenyl acceptors in the phospholipid monolayer at the surface of the human low-density lipoprotein (LDL) particle.

2. MODELS FOR DONOR AND ACCEPTOR ASSEMBLIES

In order to make the analysis of RET between the donor (D) and acceptor (A) assemblies applicable to any D,A pair, all distances, concentrations and transfer rates are expressed as dimensionless quantities. Thus, the lengths (a, t, x, s, and ϵ, to be defined below) are normalized to R_0, the Förster distance, where R_0 is defined as the donor-acceptor separation for which the RET rate, k_T, is equal to k_D, the donor rate in the absence of any

0006-3495/90/09/665/11 $2.00

acceptors. Similarly, volumes are always given in units of R_0^3 and the (dimensionless) RET rate is defined as $k = k_T/k_D$. Accordingly, the rate of RET between a D, A pair separated by a distance R, is (Förster, 1948),

$$k = (R_0/R)^6, \tag{1}$$

and the quantum efficiency of RET, Φ_T, is

$$\Phi_T = k/(1 + k). \tag{2}$$

In the models discussed below the donors are contained within a right circular cylinder of height t and radius s, with volume $v = \pi s^2 t$ and aspect ratio $\alpha \equiv 2s/t$. The donor concentration within the cylinder does not appear in the analysis presented here, because only the *average* RET rate for all donors is measured in steady-state RET experiments. If N_A is the area concentration of acceptors (nanometers^{-2}), the dimensionless planar acceptor concentration, n_A, is defined as

$$n_A = N_A R_0^2, \tag{3}$$

where R_0 is in nanometers. In the present calculations the RET orientation factor, K^2 (Förster, 1948), is assumed to be 2/3 for all D-A pairs. This value is appropriate if the orientations of both the donor and acceptor chromophores sample all orientations in times which are short compared to their excited-state lifetimes (dynamic averaging regime) (Dale et al., 1979; Eisinger et al., 1981). While this assumption is not in general a realistic one, it is unlikely to introduce a serious error, as long as the donors are large in number and both the donors and acceptors have some orientational freedom (cf., section 7).

It should be noted that the analysis presented here is in any case only an approximate one, because the actual locations of the donors and acceptors are in general unknown. To evaluate the uncertainties this may cause, we compare two approaches for calculating the average transfer rate: In the first, the donors and acceptors are assumed to be smeared out uniformly and continuously within the cylinder and over the plane, respectively, and with this assumption it is possible to obtain analytical solutions for the energy transfer problem. In the second approach, the donors and acceptors are discrete and are positioned randomly within the cylinder and the plane, respectively. The RET rates for all donor-acceptor pairs for many random distributions of donors and acceptors are then calculated and averaged to obtain the average transfer rate. It will be seen that the transfer rates obtained for the continuum and discrete random distributions are in agreement and that the frequency distribution of k values for many random distributions provides the variance in k which is to be expected when the true locations of D and A are unknown.

3. ENERGY TRANSFER FROM A DONOR TO AN INFINITE ACCEPTOR PLANE

We first consider the case of a single donor, D, at a normal (dimensionless) distance x from an infinite acceptor plane. If the normal intercepts the acceptor plane at a point C and z is the distance between D and all points of a circle of radius y, centered on C, then,

$$z^2 = x^2 + y^2. \tag{4}$$

The RET rate from D to acceptors in an area element of a circular annulus of radius y and width dy, centered on C and defined by the azimuthal angles θ and θ dθ, is, according to Eq. 1,

$$dk = n_A z^{-6} y\, dy\, d\theta. \tag{5}$$

Integrating over the entire acceptor plane, the RET rate from the donor to all acceptors is, therefore,

$$k = n_A \int_0^\infty \int_0^{2x} \frac{y\, dy\, d\theta}{(x^2 + y^2)^3} = \left(\frac{\pi}{2}\right) n_A x^{-4}. \tag{6}$$

The rate of RET from a donor a normal distance R_0 from to an infinite acceptor plane with $n_A = 1$, is, therefore, $k = \pi/2$. Note that this is ~50% greater than the RET rate between a donor and an acceptor separated by R_0 (cf., Eq. 1).

4. ENERGY TRANSFER FROM A DONOR CYLINDER TO AN ACCEPTOR PLANE

We next consider the RET from a uniform donor distribution confined to a right cylinder to an acceptor plane which is parallel to the cylinder base. We deal separately with cylinders which do not and do penetrate the plane (cf., Fig. 1).

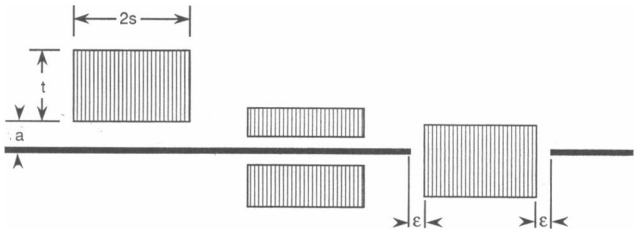

FIGURE 1 Relative locations of the donor cylinder and the acceptor plane (*heavy solid line*) for models 1a, 1b, and 2.

Model 1a: donor cylinder on one side of acceptor plane

According to Eq. 6, the rate of RET from donors within a slab of the cylinder of thickness dx is $dk = \pi^2 n_A s^2 / 2v\,(dx/x^4)$. To obtain the average rate for all donor elements within the cylinder, dk is integrated over the height (t) of the cylinder (cf., Fig. 2):

$$k = \frac{\pi^2 n_A s^2}{2v} \int_a^{a+t} x^{-4}\,dx = \frac{\pi n_A}{6t}\left[\frac{1}{a^3} - \frac{1}{(a+t)^3}\right], \quad (7)$$

where a is the normal distance between the plane and the proximal base of the cylinder.

k is seen to be proportional to the acceptor density, and whereas, it is a function of the cylinder's height and its separation from the acceptor plane, it is independent of the area or indeed the *shape* of the base of the cylinder, which was arbitrarily assumed to be circular in Eq. 7. The dependence of the transfer rate on a and t is shown in Fig. 2.

In applying Eq. 7 in the analysis of a specific protein, its volume v may be estimated from the molecular weight and the specific volume of protein. t may then be expressed in terms of the cylinder's radius, volume, and aspect ratio:

$$t = [4v/\pi\alpha^2]^{1/3}. \quad (8)$$

With Eqs. 7 and 8, the RET rate from a donor cylinder may therefore be expressed as a function of v and α.

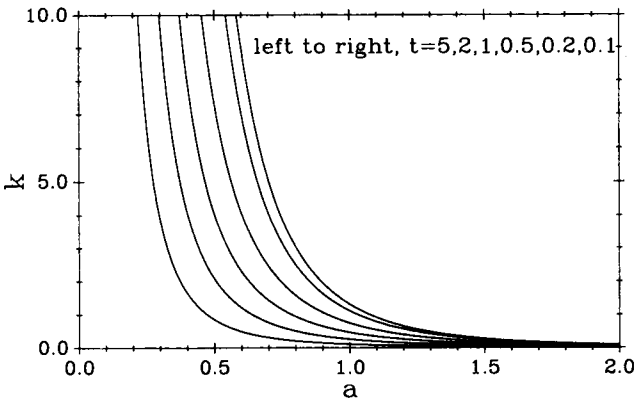

FIGURE 2 The (dimensionless) rate of RET, k, from a uniform cylindrical donor distribution to an infinite acceptor plane, as a function of a, the normal distance between the plane and the proximal cylinder base, for different values of t, the cylinder height, according to Eq. 7. All distances are in units of R_0 and the acceptor density, n_A, is unity.

Model 1b: donor cylinder on both sides of acceptor plane

This case can again be solved analytically, but only if there is no spatial overlap between the donors and acceptor distributions, because this would introduce a singularity in our mathematical model. It is therefore necessary to postulate a gap between the acceptor plane ($x = 0$) and the proximal faces of the cylinders on each side of the plane. The total RET rate from both portions of the cylinders of height t_1 and t_2, respectively, is given below. If the proximal bases of the two portions are a distance ϵ from the acceptor plane, the average RET rate is

$$k = \frac{\pi^2 n_A s^2}{2v}\left[\int_{-t_1-\epsilon}^{-\epsilon} x^{-4}\,dx + \int_{+\epsilon}^{\epsilon+t_2} x^{-4}\,dx\right] = \frac{\pi n_A}{6t}\left[\frac{2}{\epsilon^3} - \frac{1}{(t_1+\epsilon)^3} - \frac{1}{(t_2+\epsilon)^3}\right]. \quad (9)$$

Note that as in model 1a, the RET rate is independent of the *shape* of the (right) cylinder's base.

Model 2: donor cylinder penetrates concentric hole in acceptor plane

In this case the donors are distributed uniformly and continuously in the right *circular* cylinder and, for the reason stated above, the infinite acceptor plane is assumed to be free of acceptors in a concentric circular area of radius $s + \epsilon$.

To obtain the RET rate it is necessary to evaluate the average value of the inverse sixth power of all distances between a volume element of the donor cylinder, $r_D dr_D d\theta_D\,dx$, and the area element of the acceptor plane, $r_A dr_A d\theta$. Here r and θ are the cylindrical coordinates with the subscripts D and A denoting donor and acceptor. The distance, z, between these elements is then (cf., Fig. 3),

$$z^2 = x^2 + r_D^2 + r_A^2 - 2r_D r_A \cos(\theta_D - \theta_A) \quad (10)$$

and the average transfer rate of the donors in the cylinder is

$$k = \frac{n_A}{v}\int_{x=-a}^{t-a}\int_{\theta_D=0}^{2\pi}\int_{\theta_A=0}^{2\pi}\int_{r_D=0}^{s}\int_{r_A=s+\epsilon}^{\infty} z^{-6} r_A r_D\,dr_A\,dr_D\,d\theta_A\,d\theta_D\,dx. \quad (11)$$

The solution of this quintuple integral is given by Eq. A23 in Appendix A. There k is expressed in terms of an elliptic integral, as a function of v, ϵ, and α. k is seen to be a function of β, the fractional immersion of the cylinder in the acceptor plane, defined by $\beta \equiv a/t$, where a is the normal distance from the acceptor plane to one of the

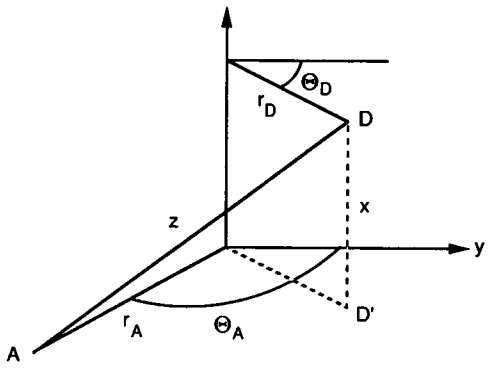

FIGURE 3 Coordinate system used to evaluate k, the RET rate, according to model 2. The acceptor element (A) lies in the acceptor plane AOy, whose orthonormal distance from the donor element (D) is $DD' = x$.

cylinder's bases. The dependence of k on β, v, α, and ϵ is illustrated graphically in Fig. 4, where n_A was set equal to unity without loss of generality, because k is always proportional to the acceptor density.

The curves of Fig. 4 show the transfer rates predicted by model 2 as a function of β, for three aspect ratios, $\alpha = 1/3$, 1, and 3. They also illustrate the strong dependence of k on ϵ, and because the value of ϵ is difficult to estimate, the model cannot be used to predict *absolute* transfer rates with confidence. On the other hand, the *relative* dependence of k on β can be used to differentiate between different geometries, because it is seen to be almost

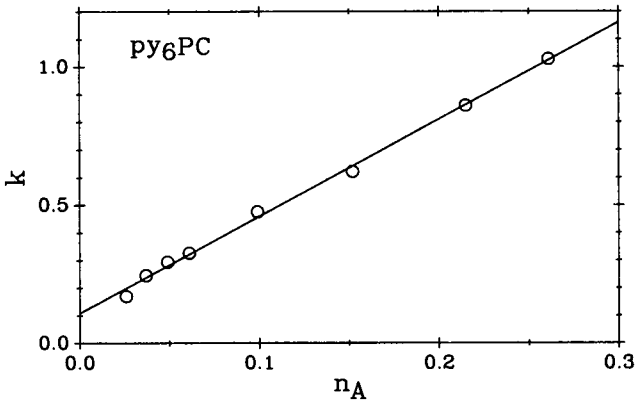

FIGURE 4 Dependence of the rate of RET from a donor cylinder to an acceptor plane penetrated by it (model 2, Eq. A23), as a function of the cylinder's fractional immersion, β, with aspect ratios $\alpha = 3$, 1, and 1/3. (*a*) $\epsilon = 0.5$, $v = 15$; (*b*) $\epsilon = 0.5$, $v = 44$; (*c*) $\epsilon = 0.25$, $v = 15$; (*d*) $\epsilon = 0.25$, $v = 44$. The curves illustrate the weak dependence of k on β, unless a base of the cylinder is nearly coplanar with the acceptors (i.e., $\beta \approx 0$ or 1), and the strong dependence of k on ϵ.

independent of ϵ. As expected, the curves of Fig. 4 are symmetrical about $\beta = 1/2$, corresponding to half of the cylinder being on each side of the acceptor plane. Note also that for small values of α, i.e., rod-shaped, as opposed to discoid donor cylinders, the transfer rate is almost independent of β, except when β is near 0 or 1.

5. RET BETWEEN RANDOMLY DISTRIBUTED DONORS AND ACCEPTORS

Because the true locations of the donor and acceptor moieties are in general unknown, it is important to consider how strongly the RET rate depends on their specific locations. To this end, we created a large number of randomly chosen distributions of donors and acceptors, and by calculating the transfer rates for all D-A pairs for each according to Eq. 1, one obtains $\langle k \rangle_{dis}$, the average for all distributions of discrete donors and acceptors. For a sufficiently large number of such computer-generated distributions (N), the frequency distribution of k values becomes independent of N, and it is clear that this limit is reached sooner when the number of donors and acceptors is large.

The following algorithm was used to create a random distribution of donors within a cylinder: Using cylindrical coordinates (r_D, z_D, θ_D), random numbers were generated to obtain values for θ_D and z_D and r_D^2 for the first donor, the radial coordinate being squared to ensure that the donors be uniformly distributed. Only those values which correspond to points within the cylinder (i.e., $r_D < s$) were retained. All donors chosen after the first are required to meet the additional condition that they be separated by a distance >0.4 nm from any previously selected donor, because that is the approximate minimum separation between aromatic residue centroids as determined from the known structures of proteins (Burley and Petsko, 1985). A similar procedure was used to select the random distributions of the acceptors, which were required to have a separation >0.8 nm, the average spacing between membrane phospholipids. Because the RET rate decreases rapidly with the D, A separation (cf., Eq. 1), transfer to acceptors whose radial distance from the cylinder perimeter was greater than $6R_0 + \epsilon$ were considered to be negligible.

Fig. 5 shows $p(k)$, the normalized probability distributions of average transfer rates (k_i) calculated for 40,000 random distributions of donors confined to cylinders with aspect ratios 1/3, 1, and 3 and acceptors in a plane, according to models 1a and 2. Their average values, $\langle k \rangle_{dis} = \Sigma p(k_i) k_i$, are listed for some representative parameters in Table 1, together with k, the transfer rates

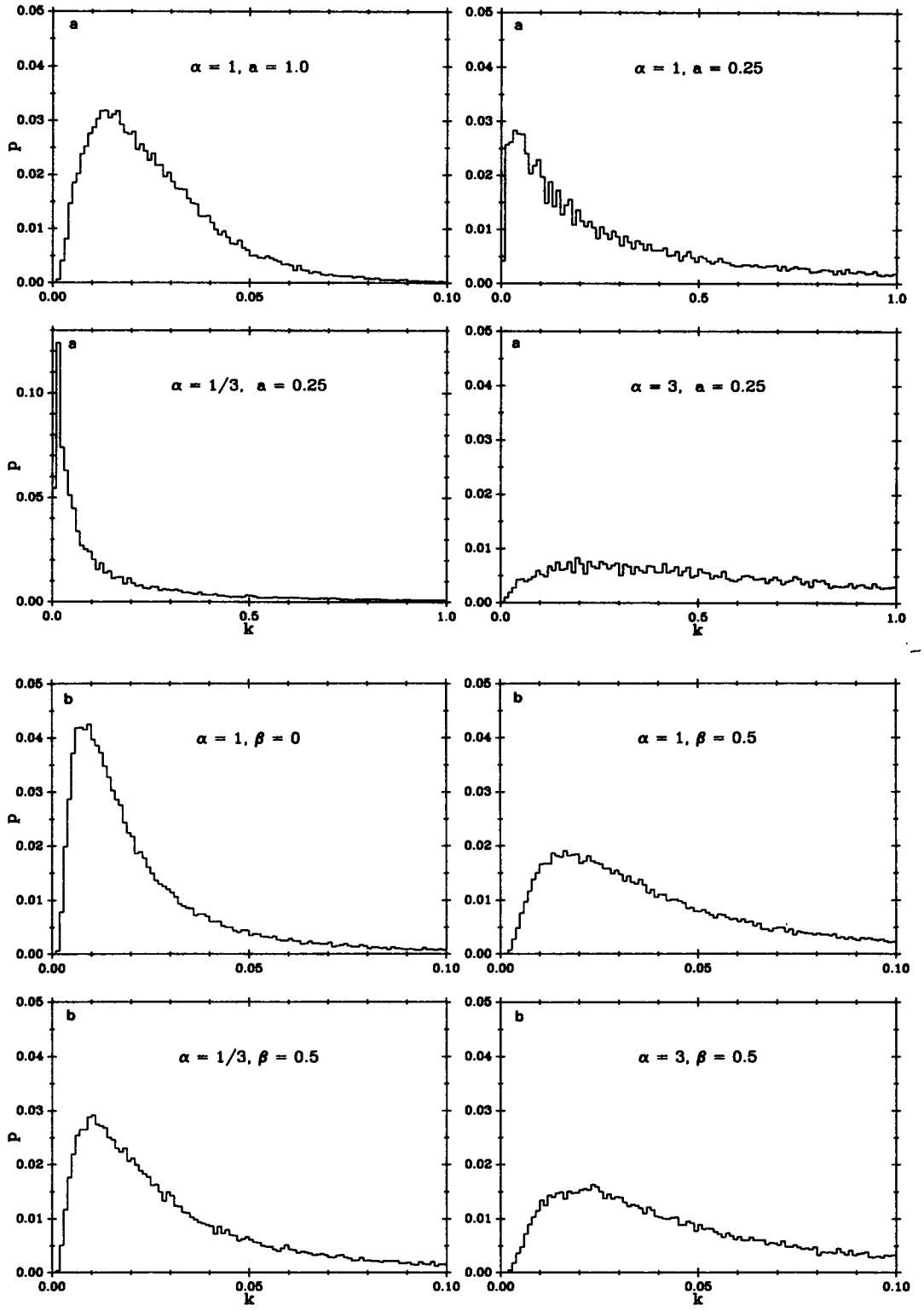

FIGURE 5 Selected normalized probability distributions of the average transfer rates, $p(k)$, for 40,000 random distributions of discrete donors and acceptors in the cylinder and plane. For each distribution of A and D positions, the transfer rates for all D, A pairs were evaluated according to Eq. 1 and averaged to obtain $\langle k \rangle_{dis}$. As in Table 1, the values of the parameters correspond to the LDL experiment discussed in section 6. (*a*) Model 1a with $a = 0.25$ and 1 and different aspect ratios. Note that when the donor cylinder is much closer than R_0 to the acceptor plane, as it is for $a = 0.25$, the distribution in k is very wide and the assumption of uniform density, as in Eq. 7 is likely to cause considerable errors. (*b*) Model 2 with $\epsilon = 0.5$. Note that the k distribution is widest for oblate donor cylinders, because of their greater circumference.

TABLE 1 **Comparison between k, the RET rate for the continuum models, and $\langle k \rangle_{dis}$, the average rate for 40,000 random distributions of discrete donors and acceptors**

α	$2s, t$	a	k	$\langle k \rangle_{dis}$
Model 1a				
1/3	8.0, 2.6	0.25	0.842	0.836
		1.0	0.013	0.012
1	3.8, 3.8	0.25	1.751	1.542
		1.0	0.027	0.026
3	1.8, 5.5	0.25	3.637	3.111
		1.0	0.054	0.048
Model 2		β		
1/3	8.0, 2.6	0	0.021	0.021
		0.5	0.042	0.043
1	3.8, 3.8	0	0.030	0.028
		0.5	0.057	0.059
3	1.8, 5.5	0	0.041	0.040
		0.5	0.070	0.070

Data are shown for models 1a and 2 for a donor cylinder of the same volume ($v = 44$) as the apo-B100 protein with $n_A = 0.2$ and $\epsilon = 0.5$ (cf., section 6). The diameter and height of the cylinder for three aspect ratios is given in column 2. As expected, k for model 1a has an approximately inverse cubic dependence on a, whereas k for model 2 is about twice as great for $\beta = 0.5$ than for $\beta = 0$. Whereas the agreement between k and $\langle k \rangle_{dis}$ is excellent, Fig. 5 shows that the distributions in k for random D, A locations are unacceptably wide for cases in which donors are in close proximity to the acceptor plane, as for $a = 0.25$ in model 1a.

for the corresponding uniform distributions, as determined by Eqs. 7 and A23. The acceptor density for all cases was $n_A = 0.2$, corresponding to a probe/lipid ratio of ~5% within the phospholipid matrix and the volume (44) and number of donors (37) are those which apply to the apo-B100 protein on the LDL particle, as discussed in section 6. Note that the excellent agreement between the rates obtained from the analytical solutions for uniform distributions (k) and $\langle k \rangle_{dis}$.

The probability distributions of Fig. 5 are asymmetrical with the value of $\langle k \rangle_{dis}$ in all cases exceeding the rate for which $p(k)$ has its maximum value, i.e., the rate corresponding to the most frequently encountered donor and acceptor distributions. The long tails of the probability distributions which are responsible for this represent RET between D, A pairs at or near their minimum separation, i.e., a or ϵ. Comparison between the $p(k)$ histograms of Fig. 5 and the average values shown in Table 1 suggest that the assumption of uniform donor and acceptor density is unlikely to introduce errors greater than a factor of 2 for aspect ratios of unity or less, but that this error can be considerably greater for cylinder-plane geometries which are very sensitive to the specific location of the donors and acceptors, for example in model 1a, in which the cylinder is in close proximity to the acceptor plane (e.g., $a = 0.25$).

6. LOCATION OF APO-B100 PROTEIN ON THE LDL PARTICLE

In this section we illustrate how RET experiments may be used to distinguish between different geometries of the donor and acceptor assemblies by analyzing a study of the human LDL particle. The experimental details, including the method used to insert the acceptor probes by the use of the phosphatidylcholine-specific transfer protein, are published elsewhere (Vauhkonen and Somerharju, 1989).

Experimental data

The LDL particle is quasispherical in shape with a diameter of 25 nm. Its core consists of neutral lipids and its surface is formed by a phospholipid monolayer which contains 50 mole percent of cholesterol (Shen et al., 1977; Goldstein and Brown, 1977). The particle carries a single receptor protein, apo-B100, whose molecular weight is 512,000 and which contains 37 tryptophan residues. The location of this unusually large protein within the LDL particle is unknown, but its apolar segments are thought to be associated with the phospholipid monolayer at the particle's surface (Knott et al., 1986; Yang et al., 1986; Olofsson et al., 1987).

Vauhkonen and Somerharju labeled the lipid monolayer with a series of pyrenyl phosphatidylcholine probes, py_nPC, whose pyrene moiety is covalently linked to the terminal carbon of molecule's *sn*-2 acyl chain, of n methylene groups in length. They then measured the efficiency of RET from the tryptophan residues of the apo-B100 protein to the acceptor probes, as a function of acceptor concentration, n_A. From the emission spectrum of tryptophan and the absorption spectrum of py_nPC the Förster distance was determined to be $R_0 = 2.5$ nm (Vauhkonen and Somerharju, 1989). The level within the phospholipid monolayer where the pyrene moieties are located was estimated from the efficiency with which their fluorescence was quenched by brominated phospholipids. In doing so, a length of 0.095 nm per methylene unit was used, this value having been determined previously for brominated phospholipid vesicles in an x-ray diffraction experiment (Lewis and Engelman, 1983; McIntosh and Holloway, 1987).

Table 2 lists the estimated depth (d) of the pyrene moieties for the five pyrenyl acceptor probes, together with the measured average RET rates (k), normalized to an acceptor concentration of $n_A = 1$. These values of k for each acceptor and at each acceptor concentration were derived from the measured RET efficiency, Φ_T, according to the relationship (cf., Eq. 2),

$$k = \frac{\Phi_T}{1 - \Phi_T}. \tag{12}$$

TABLE 2 **Experimentally determined rate of RET (k) in dimensionless units for a series of pyrenyl acceptors at different levels in the phospholipid monolayer**

Probe	Probe depth (d)		k ($n_A = 1$)
	nm	R_0 units	
py_6PC	0.81	0.32	3.61
py_8PC	0.99	0.40	3.85
$py_{10}PC$	1.17	0.47	3.43
$py_{12}PC$	1.35	0.54	2.85
$py_{14}PC$	1.53	0.61	2.65

The "depth" of the pyrene moieties below the phospholipid headgroups (d) was estimated from quenching experiments as described in the text and is given in columns 2 and 3 in nanometers and in R_0 units ($R_0 = 2.5$ nm). Column 4 gives the transfer rates k for an acceptor concentration (n_A) of unity, and was obtained by extrapolating the linear dependence of k on n_A for each of the probes (cf., Fig. 6).

When plotted against n_A, the expected linear dependence of k on n_A was obtained, and is illustrated for py_6PC in Fig. 6, and the value of k corresponding to $n_A = 1$ was obtained by extrapolation.

Note that the straight line in Fig. 6 does not pass through the origin, i.e., that the slope dk/dn_A is greater for very small acceptor densities ($n_A < 0.025$) than the slope of the line shown. This is probably due to the fact that the apo-B100 protein possesses a small number of high affinity sites for the pyrenyl acceptors and that transfer to them more efficient than to the randomly distributed acceptors (Vauhkonen and Somerharju, 1989), as has also been reported for other membrane proteins (Jones and Lee, 1985).

In Table 2, the depths of the pyrene moiety below the phospholipid headgroups for the py_nPC probes are given in nanometers and in units of R_0 using $R_0 = 2.5$ nm. This value for R_0 was calculated from the tryptophan emission and pyrene absorption spectra, with $K^2 = 2/3$ (Förster, 1948). The volume of the donor distribution, derived from the molecular weight of apo-B100 and the specific volume of proteins (0.74 ml/g), is $v = 44\ R_0^3$ units (i.e., $v = 44$).

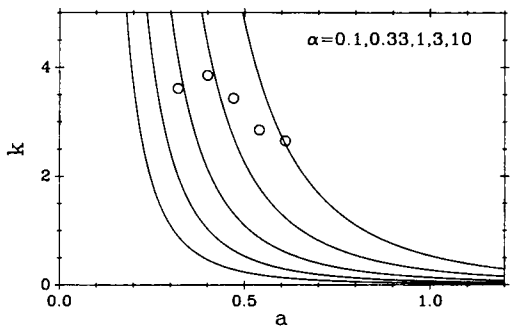

FIGURE 6 The experimentally determined dependence of the average rate of RET from the tryptophan residues in apoB-100 to py_6PC acceptors in the phospholipid monolayer of the LDL particle, on n_A, the acceptor concentration. The linear relationship is in accord with both model 1a and 2 (Eqs. 7 and 11).

Comparison of experiment with model 1a

In Fig. 7 the observed dependence of k on probe depth is compared with the predictions of model 1a according to Eq. 7, with the experimental data normalized to $n_A = 1$. The curves were generated for five values of the aspect ratio, α, for a fixed volume of $v = 44$, by making use of Eq. 8.

If the proximal face of the donor cylinder is a distance c above the phospholipid headgroup level and d is the probe depth below that plane (cf., Table 2), then $a = c + d$. (c may be negative but because the acceptor plane cannot penetrate the protein, $c > -d$). In Fig. 7 the experimental transfer rates are plotted as a function of a, which equals d when $c = 0$, i.e., when the cylinder base is coplanar with the phospholipid headgroup level. If c differs from 0, the points shown in the figure are displaced to the left (for $c < 0$) or to the right (for $c > 0$) by the magnitude of c. It is clear from Fig. 7 that the experimental dependence of k on d is much weaker than that predicted by model 1a, independently of c or α.

Comparison of experiment with model 2

The considerations above suggest that significant portions of the apo-B100 protein penetrate deeply into the phospholipid monolayer, for only then can the weak dependence of k on probe depth be explained. For that case an increase in RET from donors in the one portion compensates for the decrease from donors in the other. In this section we demonstrate that the dependence of k on d which is predicted by model 2 is indeed consistent with the observed RET rates for acceptor probes at different depths.

To compare the observed dependence of k on probe depth (cf., Table 2) with the predictions of models 1a and 2 directly, we compared the optimum fits of Eqs. 7 and A23 to the data in Fig. 8. For model 2, the immersion depth of the cylinder were expressed as $\beta = (c + d)/t$ and the values of the unknown parameters (c, α, ϵ) were obtained from the best nonlinear least square fit to the data points. As explained in the caption to Fig. 8, the quality of fit was found to be 10 times better for model 2 than for model 1a.

Whereas Fig. 8 indicates the superiority of model 2, this conclusion should not be accepted without some

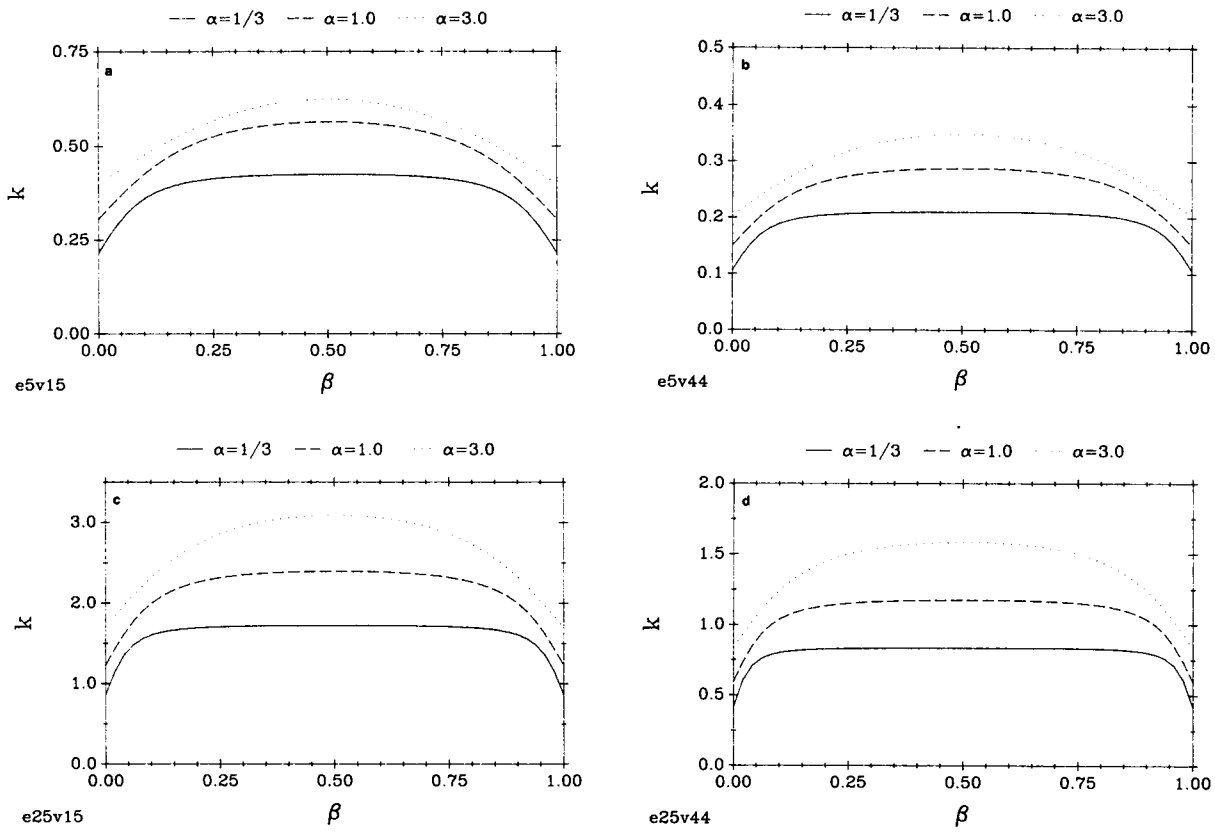

FIGURE 7 Comparison between the experimentally determined average RET rates from the tryptophan residues of apoB-100 to a series of acceptors, py_nPC with $n = 6, 8, 10, 12$, and 14 (circles, from left to right), and the k dependence predicted by model 1a. The theoretical curves for aspect ratios $\alpha = 0.1, 0.33, 1, 3$, and 10 (from left to right) were obtained by use of Eq. 7. In plotting the experimental k values, a was set equal to d, the probe depths of Table 2, i.e., with the assumption that $c = 0$ so that the base of the donor cylinder is coplanar with the phospholipid headgroups. For all other cases, the points are displaced laterally by the distance c. Note that whatever is the magnitude of c, the experimental points have a much weaker dependence on probe depth than is predicted by model 1a.

significant caveats: First, a mixture of the two models, corresponding to much of the protein being outside the phospholipid layer with some portions penetrating it, is likely to provide as good a fit as model 2. Second, another way of improving the agreement of experiment with either model is to consider the apo-B100 protein consisting of several domains with the same total volume ($v = 44$), since this would provide the donors with greater access to acceptors located between these domains. However, these and similar modifications of the two basic models considered here yield improved fits to the data at the price of introducing additional model parameters.

In summary, the results indicate that the apo-B100 protein is partially immersed in the surface of the LDL particle and probably consists of several distinct domains. The possibility that the protein lies wholly outside the phospholipid monolayer can be discounted.

7. DISCUSSION

The most important result of our analysis is that the RET efficiency from a donor assembly located one side of an acceptor plane (model 1a) has a much greater dependence on its separation from the plane than does a donor assembly which pierces the acceptor plane. By employing acceptor probes which are located at different levels of a phospholipid layer, the experimenter is in effect able to vary the separation between the donors and acceptors and draw conclusions about their relative location, as is illustrated in section 6.

A fundamental assumption in deriving the analytical results of Eqs. 7 and A23 is the uniformity of the donor and acceptor distributions. The magnitude of the error introduced by it depends, of course, on the true donor locations in an experiment but may be estimated from the

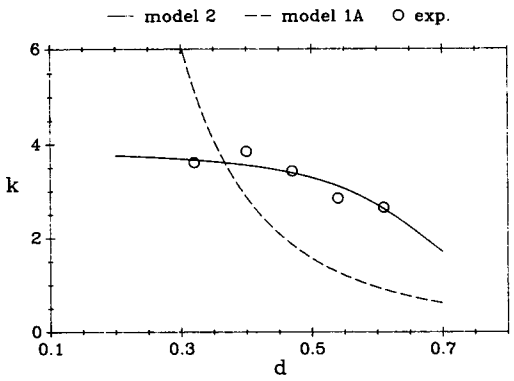

FIGURE 8 Comparison between the measured dependence of k on the probe depth, d, and the optimal fit obtained by varying the parameters of models 1a and 2. For model 1a, α was varied between $1/3$ and 3 and the best fit was found with $c = 0.052$ (~0.1 nm). For model 2, α was varied between $1/2$ and 2, c from $t - d$ to $-d$, and ϵ between 0.1 and 1. Note that c is measured from the phospholipid head group plane and is negative if the base of the cylinder is between it and the acceptor plane ($0 < c < -d$). If $c < -d$ or $c > t - d$, model 1a applies. The best fit to model 2 is obtained with $c = 3.15$, $\epsilon = 0.14$, and $\alpha = 1.0$, so that $t = 3.8$. Note, however, that this solution is not unique and that virtually the same quality of fit is found with the following three different sets of parameters: $\alpha = 0.5$, $c = 5.4$, $\epsilon = 0.121$; $\alpha = 2$, $c = 1.75$, $\epsilon = 0.150$; $\alpha = 1.7$, $c = 2.0$, $\epsilon = 0.147$. The root-mean-square error, $\Omega = [\Sigma(k_{Model} - k_{exp})^2]^{1/2}$, is a measure of the quality of the fit between model and experiment. Its magnitude is $\Omega = 3.4$ for the optimal fit with model 1a, with any of the parameter sets listed for model 2 providing a much better fit ($\Omega = 0.4$). Note that the best fits for model 2 make use of the curvature near $\beta = 0$ and 1, at the ends of the curves shown in Fig. 4. Fitting the data points with a horizontal line yields $\Omega = 1.0$ and corresponds to the assumption that the acceptor plane is near the middle of the donor cylinder so that k is almost independent of probe depth. In that case, the shape of the donor cylinder is indeterminate.

probability distributions for randomly distributed discrete donors and acceptors which are illustrated in Fig. 5. The errors are likely to be serious primarily when the number of donors is very small or when very high rates of transfer are possible, e.g., when model 1 applies and the distance a is small (cf., Fig. 5 *a*). In other cases, the error is unlikely to exceed a factor of 2, and it should still be possible to distinguish different geometries on the basis of the RET rate dependence on acceptor probe depth.

Other reasons why the assumption of uniform donor density in a protein may be inappropriate are (*a*) that the donors differ greatly in their fluorescence yields, and (*b*) that they occur in clusters. The first can be a significant source of error if the number of donors is small, since in the case of tryptophan, excited state lifetimes (and therefore their fluorescence yields) span an order of magnitude. That the second possibility is remote is suggested by a survey of tryptophan coordinates in proteins of known structure, which provides no evidence for the existence of such clusters (Burley and Petsko, 1985).

Whatever their distributions, it is clear that only donors which are within approximately one Förster distance of the donor assembly's perimeter can transfer their energy efficiently to the acceptors. The average transfer rate, k, is therefore small if the dimensions of the donor assembly greatly exceed $2R_0$, assuming that the aspect ratio of the donor cylinder is of order unity. If appreciable transfer is observed for such large donor assemblies (with $v > 10$, say), the donor assembly is likely to consist of several domains because that would permit efficient energy transfer to acceptors located between the domains.

Our simplified models for testing geometrical relationships between donor and acceptor assemblies raise the question of the error introduced by the use of the dynamical average value for the orientation factor. In the absence of specific information, it is usual to assume that $\langle K^2 \rangle = 2/3$, i.e., that the orientations of all D and A transition moments are averaged completely in times short compared to the decay and transfer times so that the dynamic averaging regime applies (Dale et al., 1979). Whereas these conditions are rarely satisfied, it can be argued that for a large number of donors and acceptors with no systematic correlations between them, the isotropic assumption is unlikely to cause serious errors in the present analysis. Suppose for example that the dynamic averaging conditions apply only partially and that while the donor has rotational freedom, the acceptor is immobile (or vice versa). In this case, K^2 may have values between $1/3$ and $4/3$, depending on the angle between the fixed transition moment and the D-A separation vector (Eisinger et al., 1981). Because of the inverse sixth power dependence of k on R_0, this range of K^2 values introduces an uncertainty of only 12% in $R_{2/3}$, the D-A separation calculated with $K^2 = 2/3$. Also, for a completely immobile D, A pair, $\langle K^2 \rangle$ can range between 0 and 4, with values near 0 introducing the greatest error in $R_{2/3}$. For random orientations of D and A, $\langle K^2 \rangle$ values near 0 occur with the greatest frequency with 8% of the $\langle K^2 \rangle$ values lying between 0 and 0.01. Nevertheless, for a D, A pair with $\langle K^2 \rangle = 0.01$ (an unlikely occurence if fluorophores retain some mobility), $R_{2/3}$ is in error by only a factor of 2 compared to the true A-D distance (Dale, 1988). The error in the *average* RET rate introduced by the dynamic averaging assumption for many donors and acceptors is likely to be much smaller.

APPENDIX

To evaluate the rate of RET (k) from a donor cylinder as a function of its fractional immersion in the acceptor plane (β), it is necessary to evaluate the quintuple integral of Eq. 11. The radial and angular

coordinates for the donor and acceptor distributions are illustrated in Fig. 3.

By defining the lumped coordinates,

$$\theta = \theta_D - \theta_A \tag{A1}$$

$$u = x^2 + r_A^2 + r_D^2 \tag{A2}$$

$$w = -2r_D r_A. \tag{A3}$$

Eq. 11 may be rewritten as the quintuple integral

$$k = \frac{n_A}{v}\int_{x=-a}^{t-a} dx \int_{r_A=s+\epsilon}^{\infty} r_A\, dr_A \int_{r_D=0}^{s} r_D\, dr_D \cdot \int_{\theta_A=0}^{2\pi} d\theta_A \int_{\theta=-\pi}^{\pi} \frac{d\theta}{(u + w\cos\theta)^3}. \tag{A4}$$

I_θ, the integral over θ in Eq. A4, may be evaluated by use of a dummy variable for $\tan(\theta/2)$ to obtain

$$I_\theta = \frac{\pi}{2}\left[\frac{1}{(u^2 - w^2)^{3/2}} + \frac{3(u^2 + w^2)}{(u^2 - w^2)^{5/2}}\right]. \tag{A5}$$

Substituting Eq. A5 in Eq. A4 and integrating over θ_A,

$$k = \frac{\pi^2 n_A}{v}\int_{x=-a}^{t-a} dx \int_{r_A=s+\epsilon}^{\infty} r_A\, dr_A \int_{r_D=0}^{s} \left[\frac{1}{(u^2 - w^2)^{3/2}} + \frac{3(u^2 + w^2)}{(u^2 - w^2)^{5/2}}\right] r_D\, dr_D. \tag{A6}$$

By introducing further changes in variables,

$$p = r_D^2 \tag{A7}$$

$$y = r_A^2 \tag{A8}$$

$$g = 2(x^2 - y) \tag{A9}$$

$$q = (x^2 + y)^2 \tag{A10}$$

$$X(p) = p^2 + gp + q. \tag{A11}$$

Eq. A6 becomes

$$k = \frac{\pi^2 n_A}{v}\int_{x=-a}^{t-a} dx \int_{y=(s+\epsilon)^2}^{\infty} dy \int_{p=0}^{s^2} \cdot \left[\frac{1}{[X(p)]^{3/2}} + \frac{6yp}{[X(p)]^{5/2}}\right] dp, \tag{A12}$$

which may be integrated with respect to p by making use of the following standard forms:

$$\int \frac{dp}{X\sqrt{X}} = \frac{2(2p + g)}{(4q - g^2)\sqrt{X}} \tag{A13}$$

$$\int \frac{p\,dp}{X^2\sqrt{X}} = -\frac{\sqrt{X}}{3X^2} - \frac{g}{2}\int \frac{dp}{X^2\sqrt{X}} \tag{A14}$$

$$\int \frac{dp}{X^2\sqrt{X}} = \frac{2(2x + g)}{3(4q - g^2)\sqrt{X}}\left[\frac{1}{X} + \frac{8}{(4q - g^2)}\right], \tag{A15}$$

to obtain

$$k = \frac{\pi^2 n_A}{v}\int_{x=-a}^{t-a} \frac{dx}{4x^4} \int_{y=(s+\epsilon)^2}^{\infty} \left[1 - \frac{(y + x^2 - s^2)}{[Y(y)]^{1/2}} + \frac{2x^2 s^2 (x^2 + s^2 - y)}{[Y(y)]^{3/2}}\right] dy, \tag{A16}$$

where

$$Y(y) = y^2 + 2(x^2 - s^2)y + (x^2 + s^2)^2. \tag{A17}$$

After integrating over x, the remaining integration over y is similar to that with respect to p above. Making use of the same standard forms, Eqs. A13–A15, in addition to

$$\int \frac{p\,dp}{\sqrt{X}} = \sqrt{X} - \frac{g}{2}\int \frac{dp}{\sqrt{X}}, \tag{A18}$$

one obtains the following expression for the average RET rate

$$k = \frac{\pi^2 n_A}{sv}\{F[m, (t - a)/s] + F[m, a/s]\}, \tag{A19}$$

where $F[m, \Gamma]$ is the following elliptic integral:

$$F(m, \Gamma) = \int_0^{\Gamma} \frac{(m + 1)\,dx}{M(m, x)[(m + 2)x^2 + m^2 + mM(m, x)]}, \tag{A20}$$

with

$$M(m, x) = [x^4 + 2(m + 2)x^2 + m^2]^{1/2} \tag{A21}$$

and

$$m = (\epsilon/s)[(\epsilon/s) + 2]. \tag{A22}$$

The rate k may be expressed as a function of v, α, β, and ϵ by rewriting Eq. A19 as

$$k = n_A(2\pi^7/\alpha v^4)^{1/3}\{F[m, 2(1 - \beta)/\alpha] + F[m, 2\beta/\alpha]\}, \tag{A23}$$

with

$$m = (2\pi/\alpha v)^{1/3}\epsilon[2 + (2\pi/\alpha v)^{1/3}\epsilon], \tag{A24}$$

and was plotted as a function of β in Fig. 7, *a–c*.

We thank Massimo Sassaroli for useful discussions and for his generous help in creating the illustrations.

This work was supported by National Institutes of Health grants HL21016 and R24 RR05272.

Received for publication 19 February 1990 and in final form 7 May 1990.

REFERENCES

Burley, S. K., and G. A. Petsko. 1985. Aromatic-aromatic interaction: a mechanism of protein structure stabilization. *Science (Wash. DC)*. 229:23–28.

Dale, R. E. 1988. Some aspects of excited-state emission spectroscopy for structure and dynamics of model and biological membranes. *In* Polarized Spectroscopy of Ordered Systems. B. Samori and E. W. Thulstrup, editors. Kluwer Academic Publishers, Dordrecht, FRG. 491–567.

Dale, R. E., J. Eisinger, and W. E. Blumberg. 1979. The orientational freedom of molecular probes: the orientation factor in intramolecular energy transfer. *Biophys. J.* 26:161–194.

Eisinger, J., and J. Flores. 1983. Cytosol-membrane interface of human erythrocytes: a resonance energy transfer study. *Biophys. J.* 41:367–379.

Eisinger, J., W. E. Blumberg, and R. E. Dale. 1981. Orientational effects in intra- and intermolecular long range excitation energy transfer. *Ann. NY Acad. Sci.* 366:155–175.

Eisinger, J., J. Flores, and R. M. Bookchin. 1984. The cytosol-membrane interface of normal and sickle erythrocytes. *J. Biol. Chem.* 259:7169–7177.

Förster, Th. 1948. Zwischenmolekulare Energiewanderung und Fluoreszenz. *Ann. Physik.* 2:55–75.

Goldstein, J. L., and M. S. Brown. 1977. The low density lipoprotein pathway and its relation to atherosclerosis. *Annu. Rev. Biochem.* 46:897–930.

Jones, O. T., and A. G. Lee. 1985. Interactions of pyrene derivatives with lipid bilayers and with (Ca- Mg)-ATPase. *Biochemistry.* 24: 2195–2202.

Knott, T. J., R. J. Pease, L. M. Powell, S. C. Wallis, S. C. Rall, Jr., T. L. Innerarity, B. Blackhart, W. H. Taylor, Y. Marcel, R. Milne, D. Johnson, M. Fuller, A. J. Lusis, B. J. McCarthy, R. W. Mahley, B. Levy-Wilson, and J. Scott. 1986. Complete protein sequence and identification of structural domains of human apolipoprotein B. *Nature (Lond.).* 323:734–738.

Lewis, B. A., and D. M. Engelman. 1983. Lipid bilayer thickness varies linearly with acyl chain length in fluid phosphatidylcholine vesicles. *J. Mol. Biol.* 166:211–217.

McIntosh, T. J., and P. W. Holloway. 1987. Determination of the depth of bromine atoms in bilayers formed from bromolipid probes. *Biochemistry.* 26:1783–1788.

Olofsson, S-O., K. Bjursell, K. Boström, P. Carlsson, J. Elovson, A. A. Protter, M. A. Reuben, and G. Bonjers. 1987. Apolipoprotein B: structure, biosynthesis and role in the lipoprotein assembly process. *Atherosclerosis.* 68:1–17.

Schiller, P. W. 1972. Study of adrenocorticotropic hormone conformation by evaluation of intramolecular resonance energy transfer in *N*-dansyllysine-ACTH-(1-24)-tetrakosipeptide. *Proc. Natl. Acad. Sci. USA.* 69:975–979.

Shen, B. W., A. M. Scanu, and F. J. Kezdy. 1977. Structure of human serum lipoproteins inferred from compositional analysis. *Proc. Natl. Acad. Sci. USA.* 74:837–841.

Stryer, L. 1978. Fluorescence energy transfer as a spectroscopic ruler. *Annu. Rev. Biochem.* 47:819–846.

Torgerson, P. M., and M. F. Morales. 1984. Application of the Dale-Eisinger analysis to proximity mapping in the contractile system. *Proc. Natl. Acad. Sci. USA.* 81:3723–3727.

Vauhkonen, M., and P. Somerharju. 1989. Parinaryol and pyrenyl phospholipids as probes for the lipid surface layer of human low density lipoproteins. *Biochim. Biophys. Acta. 984:81–87.*

Yang, C.-Y., S.-H. Chen, S. H. Giaturco, W. A. Bradley, J. T. Sparrow, M. Tanimura, W.-H. Li, D. A. Sparrow, H. DeLoof, M. Rosseneu, F.-S. Lee, Z.-W. Gu, A. M. Gotto, Jr., and L. Chan. 1986. Sequence, structure, receptor binding domains and internal repeats of human apolipoprotein B-100. *Nature (Lond.).* 323:738–742.